Numerical modeling of ultrasound propagation in the inner ear for sonoporation-mediated drug delivery

Fabrice Micaletti, David Bakhos, Jean-Michel Escoffre, Dapeng Li, Ayache Bouakaz, Damien Fouan

Numerical Modeling of Ultrasound Propagation in the Inner Ear for Sonoporation-Mediated Drug Delivery

Fabrice Micaletti MD[a,b*], David Bakhos MD-PhD[a, b, c, d], Jean-Michel Escoffre PhD[b*], Dapeng Li PhD[e], Ayache Bouakaz PhD[b], Damien Fouan PhD [b*]

a) ENT and Cervico-Facial Surgery Department, University Hospital Center of Tours, 2 Boulevard Tonnellé, 37044 Tours, France
b) Université de Tours, INSERM, Imaging Brain & Neuropsychiatry iBraiN U1253, 37032, Tours, France
c) Faculty of Medicine, Université de Tours, 10 boulevard Tonnellé, 37044 Tours, France
d) House Institute Foundation, 2100 W 3rd Street, Suite 111, Los Angeles, CA 90057, USA
e) Key Laboratory of Biomedical Information Engineering of the Ministry of Education, Department of Biomedical Engineering, School of Life Science and Technology, Xi'an Jiaotong University, China.

* Corresponding-authors

Fabrice Micaletti
Service d'ORL et Chirurgie Cervico-Faciale, CHU Tours, 2 boulevard Tonnellé, 37000 Tours, France
Tel: +33 247 474 785 Fax: +33 247 473 600
E-mail: fabrice.micaletti@etu.univ-tours.fr

Jean-Michel Escoffre
Université de Tours, INSERM, Imaging Brain & Neuropsychiatry iBraiN U1253, 37032, Tours, France
Tel: +33 247 366 191
E-mail : jean-michel.escoffre@inserm.fr

Damien Fouan
Université de Tours, INSERM, Imaging Brain & Neuropsychiatry iBraiN U1253, 37032, Tours, France
Tel: +33 247 366 191
E-mail : damien.fouan@univ-tours.fr

Abstract

To date, no treatment has been developed for targeted delivery to the inner ear (IE). Sonoporation, a promising drug delivery method, increases the permeability of round window membranes (RWMs), enhancing drug diffusion to the IE. A dedicated ultrasound protocol is essential to treat IE pathologies in combination with sonoporation. *In situ* acoustic pressure (AP) measurements cannot be used for RWM sonoporation because of the heterogeneous anatomy of the temporal bone. This study aimed to model ultrasound propagation in the IE to ensure adequate AP for RWM sonoporation. The impact of the position of the ultrasound probe relative to the RWM on AP as well as potential temperature increases from caused by tissue/ultrasound interaction were investigated. Using MATLAB®, a surgical procedure was simulated based on CT-scans of sheep heads (14 IEs). An ultrasound probe (12.7 mm in diameter, 1 MHz) with a degassed water-filled adapter was placed in front of the RWM. Mechanical properties, such as tissue density, sound speed, and ultrasound attenuation, were computed. ultrasound propagation was simulated using k-wave. Standing waves can double the AP locally; however, the final AP is comparable to a free water field map when accounting for microbubble-induced attenuation. The angle and distance of the probe relative to the RWM have minimal effect on the AP; the main effect is caused by centering the probe on the RWM. No significant thermal elevation was observed. The developed computational model paves the way for designing an optimal and safe ultrasound protocol for sonoporation-mediated drug delivery into the IE.

Manuscript

Sonoporation (also termed sonopermeabilization or microbubble-assisted ultrasound) is an innovative and promising drug-delivery modality[1], which relies on the combination of ultrasound with gas microbubbles. This modality allows targeted, efficient, and safe delivery of a wide range of therapeutic molecules (*e.g.*, antibiotics, chemotherapeutics, antibodies, and nucleic acids) for the treatment of several diseases while minimizing systemic side effects[2]. Sonoporation could be a relevant modality for curing inner ear (IE) disorders. However, acoustically mediated drug delivery into the IE is challenging because of the heterogeneous and complex anatomy of the IE[3]. The IE is an organ located within the petrous bone and occupies a volume of 78 mm^3. This organ is involved in hearing and balance[4]. Pathologies affecting the IE, causing disorders such as hearing loss and vertigo, are common and disabling. However, the intricate anatomy and function of the IE present hurdles for targeted drug delivery. The current systemic drug administration often proves ineffective[5]. The alternative approach involves local drug delivery, primarily through the round window membrane (RWM) and, to a lesser extent, the oval window membrane. The RWM is a thin membrane of approximately 70 μm thickness with a surface area of 2.5 mm^2. This membrane plays a crucial role in transmitting sound waves to the IE[6]. Currently, transtympanic injection is the most utilized method for the local administration of drugs in clinical practice. However, its efficacy remains uncertain owing to the potential leakage of therapeutic agents through the auditory tube[7]. This underscores the necessity for developing new, effective therapeutic solutions to restore auditory and vestibular function.

In this context, several preclinical studies have reported the feasibility of sonoporation-mediated drug delivery through the RWM on guinea pig, mouse and sheep models[3, 8, 9, 10, 11]. Sonoporation would stimulate intracellular, paracellular, and transcellular pathways, thus improving the accumulation of drugs in the IE[8]. In these preclinical studies, several approaches,

including transcanal (through the outer ear canal), transcranial (through the skull), and transmastoid (through the mastoid bone), have been exploited to deliver ultrasound waves to the IE[9]. Among these approaches, the transmastoid approach is the most common one. This approach requires a surgical procedure called a mastoidectomy, which is performed via a retroauricular incision to access the middle ear and to the RWM. Subsequently, therapeutic molecules are introduced into the middle ear, potentially with microbubbles for their delivery using sonoporation. The ultrasound probe is then placed through the mastoidectomy cavity, and the ultrasound waves are applied to the IE. Using this approach, preclinical studies have revealed considerably higher concentrations of therapeutic molecules in the endocochlear fluids compared to the concentrations when using transtympanic injection[3,9]. They have demonstrated great safety profiles for this approach, with preservation of hearing thresholds[10], minimal impact on the histological structure of the RWM[11], no toxic overheat, and no modification of the metabolomic profile of the endocochlear fluids[10]. Even if sonoporation proves to be a smart modality for drug delivery in the IE, its preclinical and future clinical applications would face several challenges. Among these challenges, the accurate control of ultrasound wave propagation and ultrasound parameters (*e.g.*, acoustic pressure, pulse repetition frequency, and exposure time) is crucial for efficient and safe delivery of therapeutic molecules into the IE[10]. Currently, the precise behavior of ultrasound waves in an environment as complex as the IE remains unknown. In addition, the influence of gas microbubbles on ultrasound propagation in such an environment is not reported. This knowledge gap can be attributed to the heterogeneous anatomy of the IE, which makes it challenging to measure acoustic pressure *in vitro* or *in vivo* in anatomical parts. To address this knowledge gap, we investigated the propagation of acoustic waves in the sheep IE using a CT-based computational model, because this animal model offers close similarities in size and dimensions to the human IE[12], thus allowing us to optimize future ultrasound protocols in our healthy[10] and diseased[13] sheep models.

Before conducting numerical simulations, straightforward experiments were performed to validate our computational model (Figure 1A). To achieve this objective, a single-element, custom-made piezoelectric transducer with a 12.7-mm diameter (0.5″), naturally focused at 27.2 mm, was used (Figure 1B). This transducer was connected to a 24 mm–long, degassed water–filled custom-made polymethyl methacrylate (PMMA) adapter. This adapter reduced the probe diameter to an aperture of 6 mm and allowed it to be positioned as close as possible to the RWM *in vivo*. By adding the adapter, the focal shift was reduced and was comparable to the RWM area. The focus point shifted to 6.5 mm from the distal end of the adapter. As previously described[14], the ultrasound probe with its adapter was positioned facing a calibrated polyvinylidene fluoride needle hydrophone (0.2 mm diameter, Precision Acoustic Ltd, Dorchester, the United Kingdom) in a custom-made PMMA tank filled with degassed water at room temperature (between 18 and 22°C) for acoustic measurements. This hydrophone was mounted on a three-axis robotic stage (DC -Motor Controller 500, Owis, Staufen im Breisgau, Germany). The probe with the adapter and the hydrophone were aligned using the robotic stage. An arbitrary waveform generator (33500B, Agilent, Santa Clara, CA) was used to generate an electrical sinusoidal signal with a central frequency of 1 MHz, a pulse repetition frequency of 10 kHz, and a duty cycle of 40%. These ultrasound settings were optimized in our previous experimental studies for *in vivo* gene and drug delivery[10, 15, 16]. The signal was then amplified using a RF power amplifier (AAP-500-0-2-6-D, AMD group, Valbonne, France) before being transmitted to the transducer. The probe was set up to achieve a peak negative pressure (PNP) of 300 kPa at the focus area. This acoustic pressure was chosen in agreement with the published results on the drug delivery into the IE[10,11]. The acoustic pressure field was measured along the longitudinal and perpendicular axes, X (ΔX = 15 mm) and Z (ΔZ = 15 mm). These measurements were recorded with an interval of 0.25 mm using an oscilloscope (TDS 3034, Tektronic, Beaverton, United States). No measurement was performed on the Y axis,

considering the axisymmetric nature of the probe. At each coordinate, the PNP was calculated from averaged hydrophone signals (n = 16 measurements). The obtained results were then analyzed using the MATLAB® software (Version R2022b, The MathWorks, Natick, MA, USA). The computational analysis was performed using the k-wave toolbox, which exploits a pseudo-spectral space–time method based on the fast Fourier transform to simulate the temporal propagation of acoustic waves, thus enabling investigation of the interactions between waves and matter[17, 18]. The characteristics of the numerical simulations are as follows: 1) the number of points per wavelength is 10, 2) the number of points per time period is 50, and 3) the spatial dimensions of the calculations were 32 mm × 16 mm × 16 mm. The experimental results were compared with the results obtained through a three-dimensional (3D) numerical simulation using the same features as the ultrasound probe and acoustic parameters. The simulated probe was embedded in a homogeneous medium with acoustic properties of water, *i.e.*, a speed of sound (c) of 1480 m s^{-1} and a density (ρ) of 1000 kg m^{-3}. Numerical modeling, numerical simulation, and data processing were automated via a dedicated MATLAB® code using the k-wave toolbox[19]. As shown in Figure 1C and 1D, a comparison of experimental and simulated acoustic pressures is presented in pressure maps. Results indicate a great congruence in the acoustic pressure values, with a −3 dB focus area of 13.87 ± 1.12 mm^2 and 14.45 ± 0.69 mm^2 in the experimental and simulated models, respectively, considering the incertitude measurement.

----------Insert Figure 1----------

This acoustic propagation model in an unobstructed environment (*i.e.*, free water) was adapted to a 3D simulation model in a heterogeneous environment. For this purpose, seven CT scans of the temporal bones (*i.e.*, 14 IEs) of female Ile de France sheep, with an average age of 32.4 months and an average weight of 59.6 kg (PIXANIM platform, INRAE, Nouzilly, Centre Val-de-Loire, France) were acquired using a Siemens Somatom® CT equipment (Siemens

Healthineers, Courbevoie, France) under general anesthesia in agreement with the Animal Care and Regional Committee for Ethics in Animal Experiments (APAFiS code #2018112714344369) and in accordance with European Directive 2010/63/EU for animal experiments. The acquisition protocol followed the same procedure as outlined in our previous study[12]. These CT scans were processed using k-wave. The computational domain consisted of 179 × 91 × 91 grid points, covering a volume of 26.5 × 13.5 × 13.5 mm^3. The IE and middle ear were located on the right and left sides of the sheep head by an ENT clinician (F.M.). Mastoidectomy was simulated by removing the portion of the temporal bone behind the posterior part of the external auditory canal, allowing access to the middle ear and visualization of the RWM. The ultrasound probe was modeled with the exact dimensions of the adapter. It was then displayed on the CT scan and positioned at the correct angle (90°) and distance (specifically 6.5 mm) from the RWM. The RWM was selected manually (Figure 2).

----------Insert Figure 2----------

As shown in Figure 2, the pixel intensities of the CT images are proportional to the Hounsfield units (HUs). The air located in the IE was modeled as water to simplify the acoustic simulations. Acoustic parameters were assumed to be constant for water and tissue, while they were calculated for bone based on the HU values. A linear relationship between the HU values and the acoustic parameters, including the density (1) and speed of sound (2), was also assumed. The ultrasound attenuation equation included bone porosity and the acoustic absorption coefficient (3) (Figure 3) [17, 19].

$$\rho_{skull}(x,y,z) = \rho_{min} + (\rho_{max} - \rho_{min})(1-\psi) \quad (1)$$

$$c_{skull}(x,y,z) = c_{min} + (c_{max} - c_{min})(1-\psi) \quad (2)$$

$$\alpha_{skull} = \alpha_{min,skull} + (\alpha_{max,skull} - \alpha_{min,skull}) \times \psi^{0.5} \quad (3)$$

Using $\rho_{min} = \rho_{tissue} = 1030$ kg m^{-3}, $\rho_{max} = \rho_{cortical\ bone} = 1710$ kg m^{-3}, $c_{min} = c_{tissue} = 1560$ m s^{-1}, $c_{max} = c_{cortical\ bone} = 2500$ m s^{-1} [21], and porosity $\psi = 1 + \frac{HU_{max-} - HU(x,y,z)}{HU_{max} - HU_{min}}$, where HU_{max} is the maximum HU value in the CT scan corresponding to bone and HU_{min} is the minimum HU value in the CT scan corresponding to tissue[22]. All other parameters integrated into the MATLAB® code are shown in the Table S1.

----------Insert Figure 3----------

To reflect experimental reality, an additional attenuation in the middle ear corresponding to MB attenuation must be incorporated in our numerical model. Thus, *in vitro* attenuation measurements were realized with a substitution method using a Vevo MicroMarker microbubble solution (FUJIFILM® VisualSonics, Amsterdam, the Netherlands) at 2×10^7 microbubbles/mL in a saline solution (this is the microbubble concentration used for *in vivo* IE sonoporation). The same ultrasound parameters (*i.e.*, center frequency = 1 MHz, pulse repetition frequency = 10 kHz, duty cycle = 40%, and PNP = 300 kPa in free water) were applied for 3 min. The mean value of ultrasound attenuation was measured at 10 dB cm^{-1} MHz^{-1} in our experimental conditions. This value was high considering the frequency of the ultrasound probe (1 MHz), microbubble category (Vevo MicroMarker®), and microbubble concentration[14]. Unlike classical attenuation measurements, a long pulse at higher pressure and higher microbubble concentration is used. All these parameters have a substantial impact on ultrasound attenuation[23]. Different types of simulations were performed: one with the ultrasound waves propagating in a serum solution with an attenuation of 0.00036 dB cm^{-1} MHz^{-1} [22] and others with an attenuation of 10 dB cm^{-1} MHz^{-1} based on the experimental data. Each numerical simulation required approximately 12 min for completion.

Numerical modeling was performed with 14 CT scans to account for inter-individual variability. Subsequently, new modeling was performed by varying the depth (Δ = 10 mm), lateral position (Δ = 10 mm), and angle (Δ = 80°) with respect to the RWM. The results are shown in Figure 4.

----------Insert Figure 4 ----------

The numerical simulation pressure map was significantly different from that observed in free water. Indeed, elevated acoustic pressures were observed along the bony walls of the IE. A region of interest (ROI) with a 2.2-mm diameter was drawn to delimit the RWM on the pressure maps[25]. The mean PNP value (for the 14 IEs) in the ROI was 543.30 ± 48.27 kPa in a saline solution, which was almost double the initially desired pressure, *i.e.,* 300 kPa. This increase in acoustic pressure can be attributed to the occurrence of putative standing waves, which could lead to tissue damage. However, when the ultrasound attenuation of MBs (*i.e.,* 10 dB cm^{-1} MHz^{-1}) was implemented in the numerical simulation, the PNP decreased to 320.70 ± 50.23 kPa in the ROI. In conclusion, these results demonstrate that ultrasound waves reach the RWM with a relevant PNP value (*i.e.,* approximately 320.70 ± 50.23 kPa) for its sonoporation in our experimental conditions.

In addition, the effects of ultrasound probe positioning relative to the center of the RWM on the mean PNP value in the ROI were investigated by first varying the angle between the ultrasound probe and RWM. For angle incidences ≥ |25°|, the mean PNP value was 315.30 ± 26.97 kPa, demonstrating that the ultrasound probe angle has a minimal impact on the variation in the PNP within the ROI (P = 0.99, with the Kolmogorov–Smirnov test). Then, the changes in the axial positioning of the ultrasound probe of >2 mm relative to the center of the RWM induced a decrease in the mean PNP value in the ROI, *i.e.,* 176.20 ± 133.10 kPa (*versus* 360.30 ± 81.45 kPa if the axial positioning of the ultrasound probe was <2 mm to the center of the RWM, P = 0.04 with the Kolmogorov–Smirnov test), thus revealing the substantial impact of

axial positioning of the ultrasound probe on the IE for acoustically mediated drug delivery. Although the focal spot of the ultrasound probe was 6.5 mm from the adapter, a satisfactory PNP value persisted at 8.65 mm and 408.85 kPa or at 10.81 mm and 293.0 kPa (see Figure S2). Overall, these results demonstrate that the centering of the ultrasound probe on the RWM is a key parameter to consider for IE sonoporation *in vivo*.

As generally accepted, the acoustic properties of bone considerably differ from those of surrounding soft tissues. Indeed, the exposure of bone tissue to high-intensity ultrasound waves results in a significant ultrasound absorption, leading to a considerable increase in the temperature. Such temperature increments can damage the surrounding soft tissues and negatively affect the efficacy of sonoporation-mediated drug delivery. The Pennes' bioheat equation (4) was exploited to simulate the thermal increments in our experimental conditions. This equation incorporates advective heat loss owing to tissue perfusion (blood flow through tissue) and heat deposition resulting from ultrasound absorption[26, 27].

$$\rho C_t \frac{\delta T}{\delta t} = \nabla.(k\nabla T) + Q_0 + Q \qquad (4)$$

where ρ is the material density, C is the specific heat capacity (see Table S1), T is the tissue temperature, k is the thermal conductivity constant (see Table S1), Q_0 is the blood perfusion term, and Q the heat source term ($Q = \frac{\alpha p^2}{\rho c}$) that is computed by considering the local pressure (p), absorption (α), density (ρ), and sound velocity (c). Tissue perfusion was not considered in our numerical simulations because the IE is a poorly vascularized organ[3]. The thermal properties used are detailed in the Table S1. The initial temperature for different tissues and the surrounding medium was set at 37.0°C. All numerical simulations involving ultrasound-induced heating were performed over a period of 180 s, *i.e.*, the total exposure time of our sonoporation protocol. As expected, a considerable temperature increase was observed in the entire IE (Figure 5). A maximal temperature peak of 38.89°C ± 0.24°C was calculated in the

basal turn of the cochlea, while the mean temperature in the ROI was 38.36°C ± 0.28°C. This value was 38.21°C ± 0.16°C, 15 s after the sonoporation protocol ended in the ROI. However, for simulation calculations, we assumed that the temperature of the entire medium was at 37.0°C. This assumption tends to overestimate the temperature increase, given that the temperature of the microbubble solution introduced into the middle ear is closer to 20°C *in vivo*. These temperature increments agree with those published for *in vivo* scenarios[8, 9, 10]. Preclinical studies described temperature increments ranging from +0.21°C to +2.7°C *in vivo* using temperature sensors placed at the RWM or in contact with the promontory (a prominence formed by the projection of the first turn of the cochlea) a few seconds after the end of the sonoporation when employing the transmastoid approach[8, 9, 10]. Such temperature increments have not been associated with tissue damage. Nevertheless, it is important to limit the temperature increment to not counteract the efficacy of sonoporation and not affect the sensitive structures such as the facial nerve, which are susceptible to temperature changes. It is well established that increasing the temperature of the facial nerve beyond 46°C can lead to irreversible facial paralysis[28]. Notably, such a deleterious temperature threshold was not reached in our study.

----------Insert Figure 5----------

This *in silico* model has certain limitations. While it accounts for the attenuation induced by microbubbles, it does not factor in the effect of microbubble vibrations on the ultrasound field. The step size of the k-wave could be reduced to further provide simulation accuracy using GPU acceleration. While these simulation results are promising, *ex vivo* measurements are necessary for confirmation of this numerical model. However, conducting *ex vivo* measurements on the anatomical part presents challenges, as placing the hydrophone directly

opposite to the endocochlear side of the RWM can lead to the collapse of the IE walls and distortion of acoustic propagation. As a result, reliable *ex vivo* measurements are impractical. Future studies must verify the feasibility and safety of the ultrasound protocol proposed in this paper through *in vivo* experiments.

In conclusion, CT-based numerical modeling of ultrasound propagation in the IE for sonoporation-mediated drug delivery has been developed and validated to help design ultrasound settings for such applications in a sheep model. Our ultrasound parameters appear effective and safe for sonoporation-mediated drug delivery in the sheep's IE without causing undesirable temperature increases. An important factor for efficient IE sonoporation is the precise placement of the ultrasound probe relative to the RWM. Nevertheless, further *ex vivo* and *in vivo* validations are required to take into account many factors, including the influence of MB oscillations on the ultrasound field, and therefore improve our *in silico* model despite anatomical challenges. This simulation model holds potential for future development and adaptation for human application, enabling its use in IE sonoporation for the targeted delivery of therapeutics.

Supplemental material:

Table S1: Set of parameters used to run all simulations k-wave toolbox on MATLAB®.
Figure S2: Change in the PNP as a function of the distance of the adapter tip from the RWM. The focal spot is at 6.5 mm.

Highlight image: interesting figure representing the manuscript

Keywords: numerical simulation, ultrasound propagation, drug delivery, sonoporation, inner ear

Acknowledgments: The authors acknowledge J.Y. Tartu (Université de Tours, INSERM, Imaging Brain & Neuropsychiatry iBraiN U1253, 37032, Tours, France) for the design of US probe and the technical staff from PIXANIM platform (INRAE, Université de Tours, Tours, France).

Conflict of interest: The authors have no conflicts to disclose.

Funding: This work was supported, in part, by the House Foundation (D.B.), by Inserm and Université de Tours (J.-M. E, A.B., D.B., D.F.). F.M. was the recipient of funding for his research year from the University Hospital Center of Tours.

Ethics approval: The animal study protocol was approved by the French Ethics Committee of Animal Experimentation of Centre—Val de Loire (APAFiS code #2018112714344369).

Author contributions: **Fabrice Micaletti**: Conceptualization (equal); Methodology (equal); Software (supporting); Validation (equal); Formal analysis (equal); Investigation (equal); Resources (equal); Writing—original draft preparation (lead); Writing—review and editing (equal); Visualization (equal); Project administration (equal). **David Bakhos**: Conceptualization (equal); Methodology (equal); Validation (equal); Investigation (equal); Resources (lead); Data curation (equal); Writing—review and editing (equal); Supervision (equal); Project administration (equal); Funding acquisition (lead). **Jean-Michel Escoffre**: Conceptualization (equal); Methodology (equal); Validation (equal); Formal analysis (equal); Investigation (equal); Resources (equal); Data curation (equal); Writing—original draft preparation (supporting); Writing—review and editing (equal); Supervision (equal); Project administration (equal); Funding acquisition (equal). **Dapeng Li**: Software (supporting); Validation (equal); Formal analysis (equal); Resources (equal); Data curation (equal); Writing—review and editing (equal). **Ayache Bouakaz**: Writing—review and editing (equal). **Damien Fouan**: Conceptualization (equal); Methodology (equal); Software (lead); Validation (equal); Formal analysis (equal); Investigation (equal); Resources (equal); Data curation (equal); Writing—original draft preparation (supporting); Writing—review and editing (equal); Visualization (equal); Supervision (equal); Project administration (equal). All authors have read and agreed to the published version of the manuscript.

References

1. Kooiman K, Roovers S, Langeveld SAG, Kleven RT, Dewitte H, O'Reilly MA, Escoffre JM, Bouakaz A, Verweij MD, Hynynen K, Lentacker I, Stride E, Holland CK. Ultrasound-Responsive Cavitation Nuclei for Therapy and Drug Delivery. Ultrasound Med Biol. 2020 Jun;46(6):1296-1325. https://doi:10.1016/j.ultrasmedbio.2020.01.002.
2. Bouakaz A, Michel Escoffre J. From concept to early clinical trials: 30 years of microbubble-based ultrasound-mediated drug delivery research. Adv Drug Deliv Rev. 2024 Mar;206:115199. https://doi:10.1016/j.addr.2024.115199.
3. Micaletti F, Escoffre JM, Kerneis S, Bouakaz A, Galvin JJ 3rd, Boullaud L, Bakhos D. Microbubble-assisted ultrasound for inner ear drug delivery. Adv Drug Deliv Rev. 2023 Nov 30:115145. https://doi:10.1016/j.addr.2023.115145.
4. Breitsprecher TM, Pscheidl A, Bächinger D, Volkenstein S, Dhanasingh A, Van Rompaey V, Mlynski R, Dazert S, Van de Heyning P, Langner S, Roland P, Weiss NM. Cochlear and Vestibular Volumes in Inner Ear Malformations. Otol Neurotol. 2022 Sep 1;43(8):e814-e819. https://doi:10.1097/MAO.0000000000003615.
5. Glueckert R, Johnson Chacko L, Rask-Andersen H, Liu W, Handschuh S, Schrott-Fischer A. Anatomical basis of drug delivery to the inner ear. Hear Res. 2018 Oct;368:10-27. https://doi:10.1016/j.heares.2018.06.017.
6. Goycoolea MV, Lundman L. Round window membrane. Structure function and permeability: a review. Microsc Res Tech. 1997 Feb 1;36(3):201-11. https://doi:10.1002/(SICI)1097-0029(19970201)36:3<201::AID-JEMT8>3.0.CO;2-R.
7. Salt AN, Plontke SK. Principles of local drug delivery to the inner ear. Audiol Neurootol. 2009;14(6):350-60. https://doi:10.1159/000241892.
8. Lin YC, Chen HC, Chen HK, Lin YY, Kuo CY, Wang H, Hung CL, Shih CP, Wang CH. Ultrastructural Changes Associated With the Enhanced Permeability of the Round Window Membrane Mediated by Ultrasound Microbubbles. Front Pharmacol. 2020 Jan 28;10:1580. https://doi:10.3389/fphar.2019.01580.
9. Liao AH, Wang CH, Weng PY, Lin YC, Wang H, Chen HK, Liu HL, Chuang HC, Shih CP. Ultrasound-induced microbubble cavitation via a transcanal or transcranial approach facilitates inner ear drug delivery. JCI Insight. 2020 Feb 13;5(3):e132880. https://doi:10.1172/jci.insight.132880.
10. Kerneis S, Escoffre JM, Galvin JJ 3rd, Bouakaz A, Presset A, Alix C, Oujagir E, Lefèvre A, Emond P, Blasco H, Bakhos D. Sonoporation of the Round Window Membrane on a Sheep Model: A Safety Study. Pharmaceutics. 2023 Jan 29;15(2):442. https://doi:10.3390/pharmaceutics15020442.
11. Zhang Z, Chen Z, Fan L, Landry T, Brown J, Yu Z, Yin S, Wang J. Ultrasound-microbubble cavitation facilitates adeno-associated virus mediated cochlear gene transfection across the round-window membrane. Bioeng Transl Med. 2020 Oct 3;6(1):e10189. https://doi:10.1002/btm2.10189.
12. Trinh TT, Cohen C, Boullaud L, Cottier JP, Bakhos D. Sheep as a large animal model for cochlear implantation. Braz J Otorhinolaryngol. 2022 Nov-Dec;88 Suppl 1(Suppl 1):S24-S32. https://doi:10.1016/j.bjorl.2021.02.014.
13. Boullaud L, Blasco H, Caillaud E, Emond P, Bakhos D. Immediate-Early Modifications to the Metabolomic Profile of the Perilymph Following an Acoustic Trauma in a Sheep Model. J Clin Med. 2022 Aug 10;11(16):4668. https://doi:10.3390/jcm11164668.
14. Escoffre JM, Novell A, Piron J, Zeghimi A, Doinikov A, Bouakaz A. Microbubble attenuation and destruction: are they involved in sonoporation efficiency? IEEE Trans

Ultrason Ferroelectr Freq Control. 2013 Jan;60(1):46-52. https://doi:10.1109/TUFFC.2013.2536.

15. Espitalier F, Darrouzain F, Escoffre JM, Ternant D, Piver E, Bouakaz A, Remerand F. Enhanced Amikacin Diffusion With Ultrasound and Microbubbles in a Mechanically Ventilated Condensed Lung Rabbit Model. Front Pharmacol. 2020 Jan 16;10:1562. https://doi:10.3389/fphar.2019.01562.
16. Bressand D, Novell A, Girault A, Raoul W, Fromont-Hankard G, Escoffre JM, Lecomte T, Bouakaz A. Enhancing Nab-Paclitaxel Delivery Using Microbubble-Assisted Ultrasound in a Pancreatic Cancer Model. Mol Pharm. 2019 Sep 3;16(9):3814-3822. https://doi:10.1021/acs.molpharmaceut.9b00416.
17. Mueller JK, Ai L, Bansal P, Legon W. Numerical evaluation of the skull for human neuromodulation with transcranial focused ultrasound. J Neural Eng. 2017 Dec;14(6):066012. https://doi:10.1088/1741-2552/aa843e.
18. Chen M, Peng C, Wu H, Huang CC, Kim T, Traylor Z, Muller M, Chhatbar PY, Nam CS, Feng W, Jiang X. Numerical and experimental evaluation of low-intensity transcranial focused ultrasound wave propagation using human skulls for brain neuromodulation. Med Phys. 2023 Jan;50(1):38-49. https://doi:10.1002/mp.16090.
19. B. E. Treeby, J. Jaros, A. P. Rendell, and B. T. Cox, "Modeling nonlinear ultrasound propagation in heterogeneous media with power law absorption using a k-space pseudospectral method," J. Acoust. Soc. Am., vol. 131, no. 6, pp. 4324-4336, 2012.
20. Chen M, Peng C, Wu H, Huang CC, Kim T, Traylor Z, Muller M, Chhatbar PY, Nam CS, Feng W, Jiang X. Numerical and experimental evaluation of low-intensity transcranial focused ultrasound wave propagation using human skulls for brain neuromodulation. Med Phys. 2023 Jan;50(1):38-49. https://doi:10.1002/mp.16090.
21. Montanaro H, Pasquinelli C, Lee HJ, Kim H, Siebner HR, Kuster N, Thielscher A, Neufeld E. The impact of CT image parameters and skull heterogeneity modeling on the accuracy of transcranial focused ultrasound simulations. J Neural Eng. 2021 May 4;18(4). https://doi:10.1088/1741-2552/abf68d.
22. Angla C, Larrat B, Gennisson JL, Chatillon S. Transcranial ultrasound simulations: A review. Med Phys. 2023 Feb;50(2):1051-1072. https://doi:10.1002/mp.15955.
23. Sojahrood AJ, Li Q, Haghi H, Karshafian R, Porter TM, Kolios MC. Probing the pressure dependence of sound speed and attenuation in bubbly media: Experimental observations, a theoretical model and numerical calculations. Ultrason Sonochem. 2023 May;95:106319. https://doi:10.1016/j.ultsonch.2023.106319.
24. Hosseini S, Puonti O, Treeby B, Hanson LG, Thielscher A. A head template for computational dose modelling for transcranial focused ultrasound stimulation. Neuroimage. 2023 Aug 15;277:120227.https://doi:10.1016/j.neuroimage.2023.120227.
25. Han S, Suzuki-Kerr H, Suwantika M, Telang RS, Gerneke DA, Anekal PV, Bird P, Vlajkovic SM, Thorne PR. Characterization of the Sheep Round Window Membrane. J Assoc Res Otolaryngol. 2021 Feb;22(1):1-17. https://doi:10.1007/s10162-020-00778-9.
26. Pennes HH. Analysis of tissue and arterial blood temperatures in the resting human forearm. J Appl Physiol. 1948 Aug;1(2):93-122. https://doi:10.1152/jappl.1948.1.2.93.
27. Kyriakou A, Neufeld E, Werner B, Székely G, Kuster N. Full-wave acoustic and thermal modeling of transcranial ultrasound propagation and investigation of skull-induced aberration correction techniques: a feasibility study. J Ther Ultrasound. 2015 Jul 31;3:11. https://doi:10.1186/s40349-015-0032-9.

28. Dillon NP, Fichera L, Kesler K, Zuniga MG, Mitchell JE, Webster RJ 3rd, Labadie RF. Pre-operative Screening and Manual Drilling Strategies to Reduce the Risk of Thermal Injury During Minimally Invasive Cochlear Implantation Surgery. Ann Biomed Eng. 2017 Sep;45(9):2184-2195. https://doi:10.1007/s10439-017-1854-0.
29. Pasquinelli C, Montanaro H, Lee HJ, Hanson LG, Kim H, Kuster N, Siebner HR, Neufeld E, Thielscher A. Transducer modeling for accurate acoustic simulations of transcranial focused ultrasound stimulation. J Neural Eng. 2020 Jul 13;17(4):046010. https://doi:10.1088/1741-2552/ab98dc.
30. Robertson JL, Cox BT, Jaros J, Treeby BE. Accurate simulation of transcranial ultrasound propagation for ultrasonic neuromodulation and stimulation. J Acoust Soc Am. 2017 Mar;141(3):1726. https://doi:10.1121/1.4976339.
31. Montanaro H, Pasquinelli C, Lee HJ, Kim H, Siebner HR, Kuster N, Thielscher A, Neufeld E. The impact of CT image parameters and skull heterogeneity modeling on the accuracy of transcranial focused ultrasound simulations. J Neural Eng. 2021 May 4;18(4). https://doi:10.1088/1741-2552/abf68d.
32. Drainville RA, Chatillon S, Moore D, Snell J, Padilla F, Lafon C. A simulation study on the sensitivity of transcranial ray-tracing ultrasound modeling to skull properties. J Acoust Soc Am. 2023 Aug 1;154(2):1211-1225. https://doi:10.1121/10.0020761.
33. Yoon K, Lee W, Lee JE, Xu L, Croce P, Foley L, Yoo SS. Effects of sonication parameters on transcranial focused ultrasound brain stimulation in an ovine model. PLoS One. 2019 Oct 24;14(10):e0224311. https://doi:10.1371/journal.pone.0224311.

Figures:

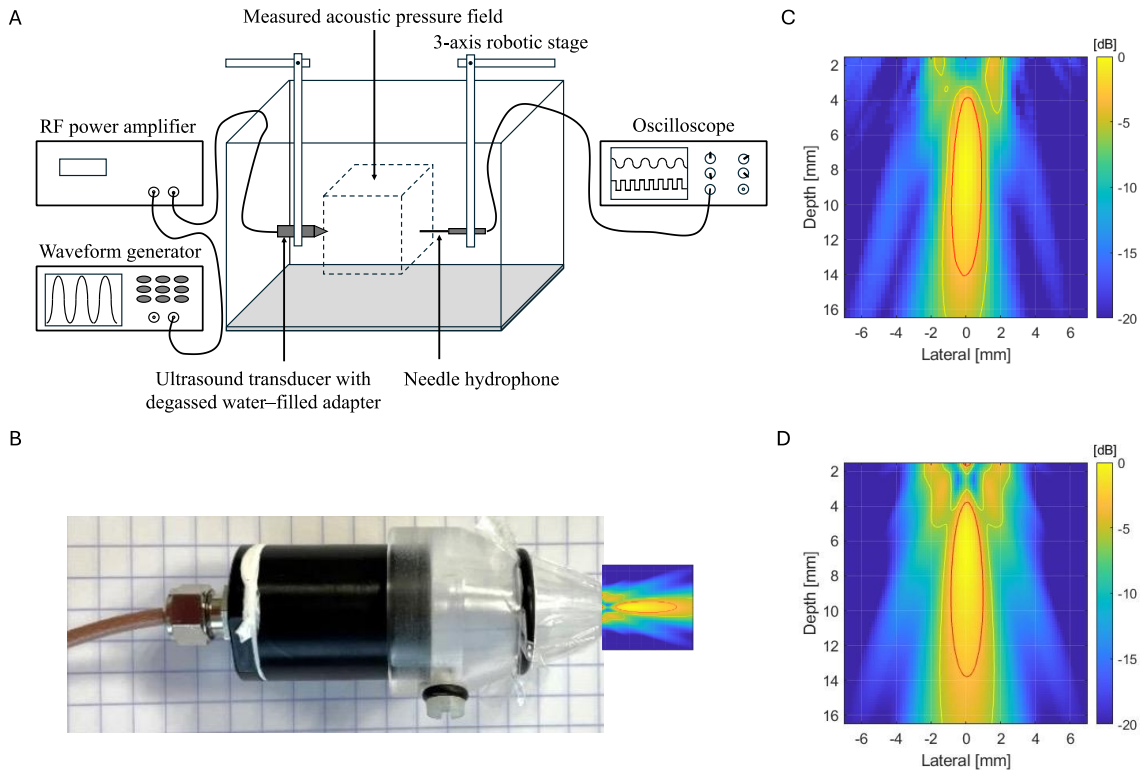

Figure 1: Validation of our model using simple experimental and computed experiments

A. Experimental experiment: the ultrasound probe, equipped with its adapter, is positioned in a tank filled with degassed water at room temperature. Opposite the probe, a needle hydrophone is mounted on a 3-axis robotic stage. The probe is connected to a waveform generator set to a center frequency of 1 MHz, a pulse repetition frequency of 10 kHz, and a 40% duty cycle. The signal is amplified via an RF power amplifier. The acoustic pressure field is measured over a cubic volume of 15 × 15 mm. All measurements are recorded on an oscilloscope and subsequently analyzed using MATLAB® software. B. Lab-made 13-mm diameter probe with a conical adapter filled with degassed water. C. Experimental ultrasound field. D. Computed ultrasound field. Results are expressed in attenuation (dB). The 0-mm depth corresponds to the tip of the adapter. The red ellipse represents the focal spot at −3 dB, and the white lines represent the focal spot at −6 dB.

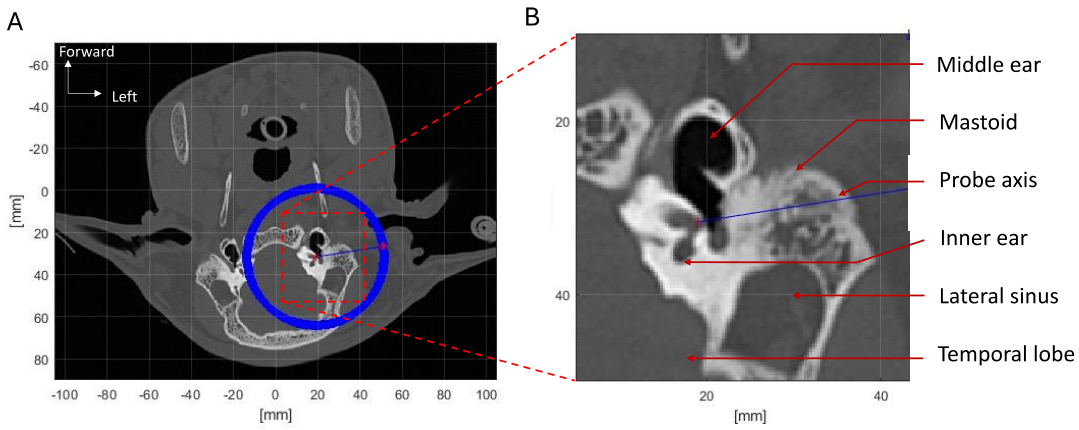

Figure 2: A. CT scan of the sheep head. The middle and inner ear of the left side are located using a blue circle. B. ROI is segmented, and the axis of the ultrasound probe is positioned perpendicular to the RWM at the lower end of the blue line.

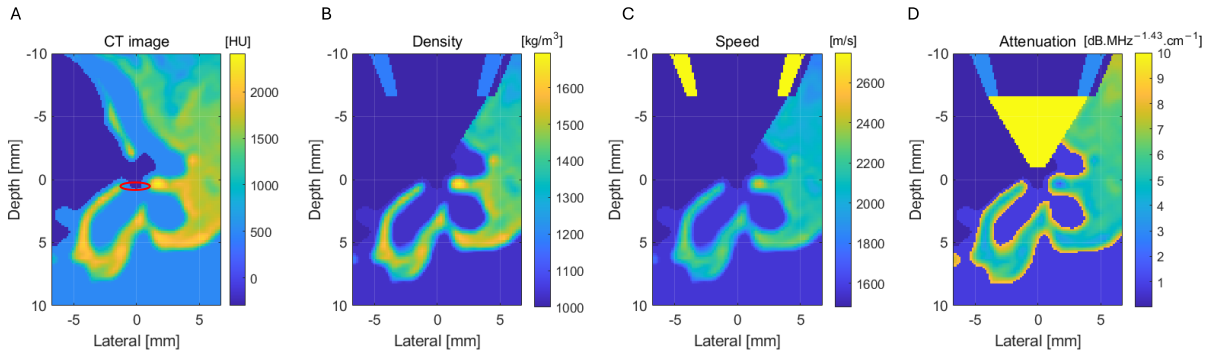

Figure 3: A. Original image of sheep's middle and inner ear. The red circle represents the ROI, the RWM. B. Density, C. Speed, and D. Attenuation calculated after mastoidectomy simulation and adapter tip positioning at 6.5 mm.

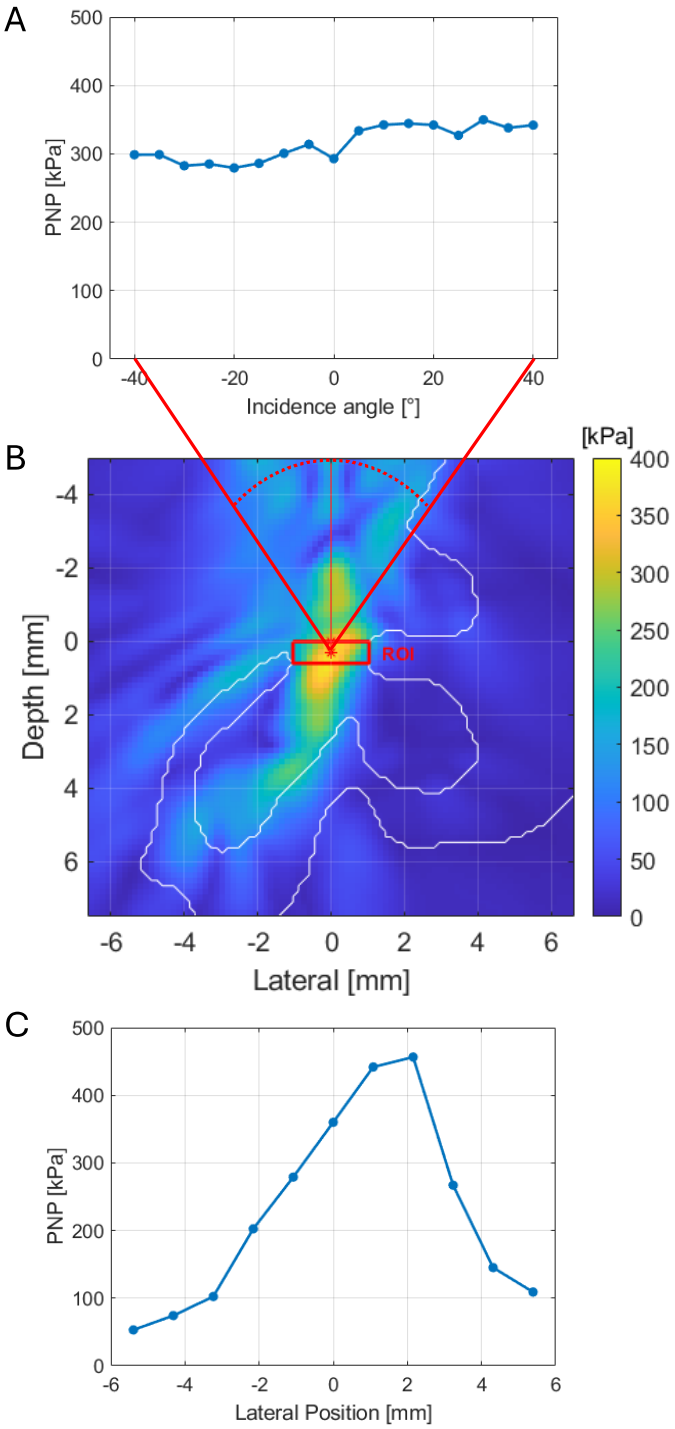

Figure 4: A. Change in the PNP as a function of the incidence angle of the ultrasound probe. B. Acoustic pressure mapping with ideal probe positioning in an microbubble solution. C. Change in the PNP as a function of the probe's lateral position relative to the center of the RWM.

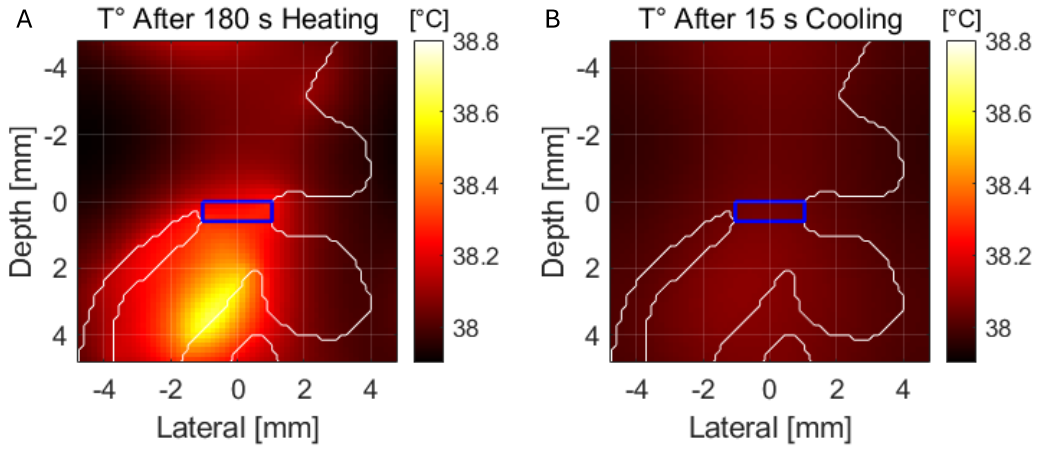

Figure 5: A. Computed temperature map of the middle and inner ear over a period of 180 s, *i.e.*, the total ultrasound exposure time. B. Computed temperature map of the middle and inner ear 15 s after the end of US exposure.

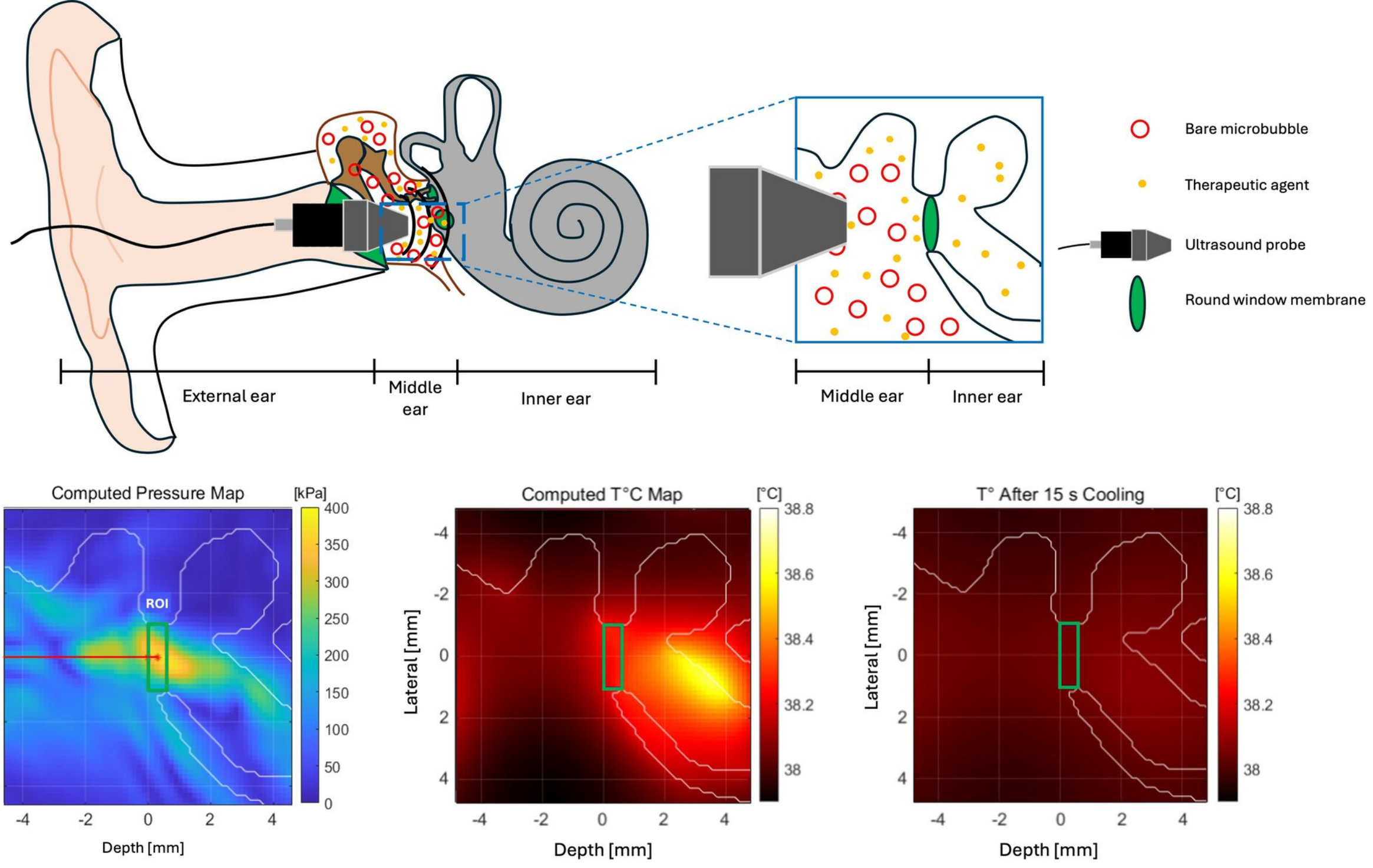
External ear
Middle ear
Inner ear
Middle ear
Inner ear
Bare microbubble
Therapeutic agent
Ultrasound probe
Round window membrane
Computed Pressure Map
[kPa]
ROI
Lateral [mm]
Depth [mm]
Computed T°C Map
[°C]
Lateral [mm]
Depth [mm]
T° After 15 s Cooling
[°C]
Lateral [mm]
Depth [mm]

Supplemental online material: Numerical Modeling of Ultrasound Propagation in the Inner Ear for Sonoporation-Mediated Drug Delivery

F. Micaletti, D. Bakhos, J-M. Escoffre, D. Li, A. Bouakaz, D. Fouan

Table S1: Set of parameters used to run all simulations k-wave toolbox on MATLAB®.

Acoustic properties of different materials	Values	Units	Reference
Water wave speed (c_w)	1 482	$m.s^{-1}$	17, 29
Soft tissue wave speed (c_t)	1560	$m.s^{-1}$	30
Cortical bone wave speed (max HU) (c_b)	2 500	$m.s^{-1}$	31
Water density (ρ_w)	1 000	$kg.m^{-3}$	24, 31
Soft tissue density (ρ_t)	1 040	$kg.m^{-3}$	30
Cortical bone density (max HU) (ρ_b)	1 710	$kg.m^{-3}$	31
Power absorption coefficient	1.43		32
Water attenuation ($\propto_w$)	0.00036	$dB.cm^{-1}.MHz^{-1}$	24
Soft tissue attenuation ($\propto_t$)	0.8	$dB.cm^{-1}.MHz^{-1}$	33
Sheep skull maximum attenuation ($\propto_b$)	8.6859	$dB.cm^{-1}.MHz^{-1}$	31
Thermal conductivity in water (κ_w)	0.615	$W.m\text{-}1.K^{-1}$	24
Thermal conductivity in soft tissue (κ_t)	0.528	$W.m\text{-}1.K^{-1}$	24
Thermal conductivity in cortical bone (κ_b)	0.32	$W.m\text{-}1.K^{-1}$	24
Specific heat in water (C_w)	4 180	$J.kg^{-1}.K^{-1}$	24

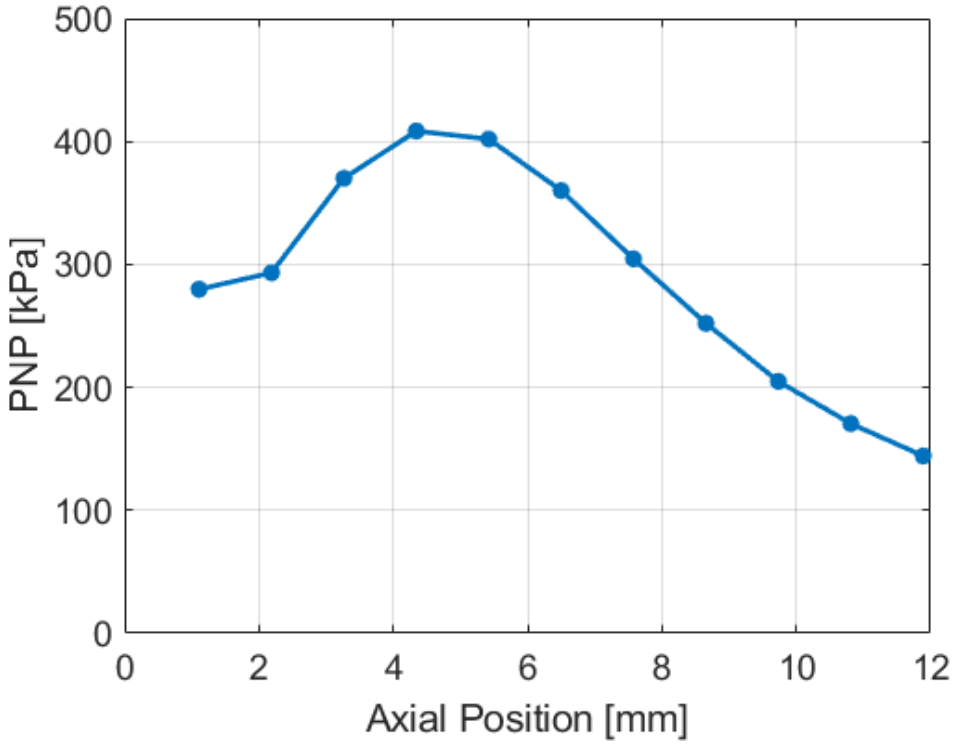

Figure S2: Change in the PNP as a function of the distance of the adapter tip from the RWM. The focal spot is at 6.5 mm.